Diffusion-limited kinetics of the solution–solid phase transition of molecular substances

Dimiter N. Petsev*, Kai Chen†, Olga Gliko*, and Peter G. Vekilov*‡

*Department of Chemical Engineering, University of Houston, Houston, TX 77204; and †Center for Microgravity and Materials Research, University of Alabama, Huntsville, AL 35899

Edited by John M. Prausnitz, University of California, Berkeley, CA, and approved November 26, 2002 (received for review May 21, 2002)

For critical tests of whether diffusion-limited kinetics is an option for the solution–solid phase transition of molecular substances or whether they are determined exclusively by a transition state, we performed crystallization experiments with ferritin and apoferritin, a unique pair of proteins with identical shells but different molecular masses. We find that the kinetic coefficient for crystallization is identical (accuracy ≤7%) for the pair, indicating diffusion-limited kinetics of crystallization. Data on the kinetics of this phase transition in systems ranging from small-molecule ionic to protein and viri suggest that the kinetics of solution-phase transitions for broad classes of small-molecule and protein materials are diffusion-limited.

The kinetics of the reactions in solutions are either limited only by the rate of diffusion of the species (1) or additionally slowed down by a transition state (2). For the kinetics of the phase transitions in solutions, it is generally accepted that colloid particles follow the diffusion-limited model, whereas the growth rates of new phases of small molecules are thought to be governed by a transition state (3–7). For the intermediate case of protein solid phases, the growth kinetics largely resemble those of small molecules, and it was assumed that transition-state laws apply (8). Although rate laws reminiscent of diffusion-limited mechanisms have been postulated for small-molecule phase transitions (9–11), they were viewed as equivalent to respective transition-state expressions (10, 11), and no critical tests to discriminate between the two mechanisms were suggested or performed.

In the transition-state kinetics, the rate coefficients are (*i*) mass-dependent (12, 13), (*ii*) independent on the diffusivity (2), and (*iii*) faster for high-symmetry molecules because of the transition-state entropy (7). Hence, for tests of the mechanism of growth of the new phase during a solution–solid phase transition, we selected the crystallization of ferritin/apoferritin, a unique pair of proteins that share a near-spherical protein shell, consisting of 24 identical subunits (14, 15). The crystals of ferritin and apoferritin are typically faceted by octahedral [111] faces and have been shown to grow by the lateral spreading of layers generated by two-dimensional nucleation (16, 17). For apoferritin, it was shown that the edges of the unfinished layers, called growth steps, propagate by the incorporation of single protein molecules at the growth sites, kinks (16, 18). In the face-centered cubic lattice that ferritin and apoferritin share, kinks are defined as the termination points of three independent ⟨011⟩ rows of molecules belonging to the unfinished layer (19). Thus, the step velocity equals the product of the molecular diameter a, mean kink density $\bar{n}_k^{-1}$, and net molecular flux into a kink $(j_+ - j_-)$ (16, 18).

Methods

Characterization of the Molecular Masses and Pair Interactions of Ferritin and Apoferritin. We performed static light scattering (20) in 0.2 M $NaOOCCH_3$ solutions. The molecular masses, M_w, and the second osmotic virial coefficients, A_2, in dimensional form were determined from the Debye plots,

$$\frac{KC}{R_\theta} = \frac{1}{M_w} + 2A_2C,$$

where R_θ is the Raleigh ratio of the scattered to the incident light intensity, K is a system constant,

$$K = \frac{1}{N_A}\left(\frac{2\pi n_0}{\lambda^2}\right)^2\left(\frac{dn}{dC}\right)^2,$$

$n_0 = 1.3320$ is the refractive index of the solvent at the wavelength of the laser beam $\lambda = 0.6328$ μm (21, 22), dn/dC is the n increment with the protein concentration, C, determined for each protein at $\lambda = 0.628$ μm by a differential refractometer (Wyatt Technology, Santa Barbara, CA). For ferritin $dn/dC = 0.290$ $cm^3 \cdot g^{-1}$; for apoferritin, $dn/dC = 0.159$ $cm^3 \cdot g^{-1}$.

Determination of the Kinetic Coefficients for Step Growth for Ferritin and Apoferritin. We determined the dependencies of the step velocities v on the crystallization driving force $\{\exp[-(\mu_c - \mu_s)/k_BT] - 1\} = (C/C_e - 1)$; subscripts c and s denote crystal and solute, respectively; subscript e denotes equilibrium. The equality is based on $\mu_s = \mu_0 + k_BT \ln(\gamma C)$, and $\mu_c = \mu_0 + k_BT \ln(\gamma_e C_e)$, with $\gamma \approx \gamma_e \approx 1$ as shown in ref. 18.

As a first method of step-velocity determination, we used sequences of molecular resolution *in situ* atomic force microscopy (AFM) images of the advancing steps as described (16, 18). The step velocities were determined as the ratio $Na/\Delta t$, where N is the number of molecular sizes a that the step advances for the time between two sequential images Δt. For each concentration of ferritin or apoferritin, ≈20 determinations of v were done and averaged. The error bars for these types of data represent the 90% confidence interval for these averages (23).

For additional step-velocity data for apoferritin, we disabled the slow scanning axis of the AFM (16). In the collected pseudoimages, the vertical axis represents time, which allowed us to monitor for times of 60–90 min with a frequency 2–4 s^{-1} the propagation of 15–30 steps within 10-μm segments of a growing crystal surface (24). For each apoferritin concentration, the average of 30–80 velocities averaged over the monitoring times was evaluated; the error bars represent the standard deviations of each sample.

As a third method, applied to ferritin, we extracted averaged values of the step velocities from time traces of this variable recorded with a frequency of 1 s^{-1} at chosen points on the growing crystal surface using laser interferometry as discussed in detail in refs. 25 and 26. Each point represents the average of ≈1,000 measurements (26, 27), and the error bar represents the 90% confidence interval for this average (23).

This paper was submitted directly (Track II) to the PNAS office.

Abbreviation: AFM, atomic force microscopy.

‡To whom correspondence should be addressed. E-mail: vekilov@uh.edu.

www.pnas.org/cgi/doi/10.1073/pnas.0333065100

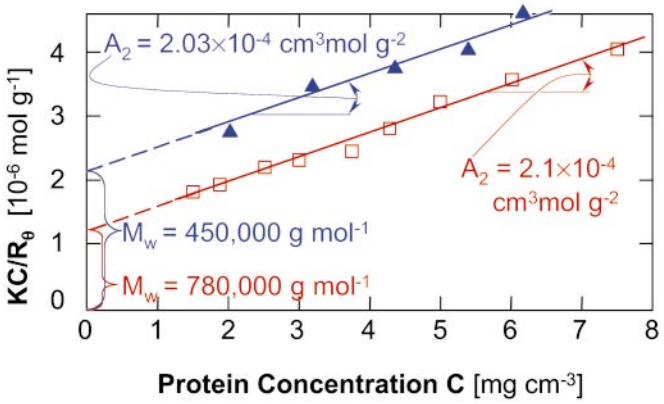

Fig. 1. Characterization of the molecular masses and pair interactions of ferritin and apoferritin. Debye plots of the scattered intensity determined in a static light-scattering experiment as a function of the concentration C of the two proteins in solutions in 50 mM NaAc buffer. The molecular masses, M_w, and the second osmotic virial coefficients in the dimensional form, A_2, of the two proteins are shown in the plot.

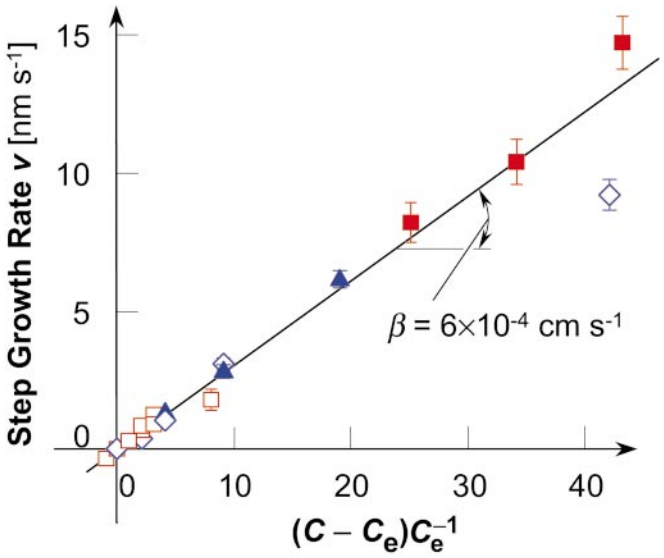

Fig. 2. Determination of the kinetic coefficients for step growth for ferritin and apoferritin: Dependencies of the step growth rates v on the crystallization driving force $(C/C_e - 1)$. □ and ◇, v values for ferritin and apoferritin, respectively, from sequences of molecular resolution *in situ* AFM images of the advancing steps. The reason for the lower value of the point for apoferritin at $(C/C_e - 1) = 42$ is not well understood. This point was not used in the determination of the kinetic coefficient β. ▲, data for apoferritin extracted from disabled y-axis scans; ■, data for ferritin from time traces of the step growth rate by using laser interferometry; straight line, the step kinetic coefficient $\beta = 6 \times 10^{-4}$ cm·s^{-1} from refs. 16 and 18.

Results and Discussion

The molecular mass (M_w) of apoferritin has been determined by many techniques to be 450,000 g·mol^{-1} (14, 15), with the mass of a molecule $m = 7.47 \times 10^{-19}$ g. However, the average M_w of ferritin varies between 550,000 and 950,000 g·mol^{-1} depending on the size of the ferrite core (14, 15). To determine the M_w of ferritin in the samples used here, we used static light scattering (20). The Debye plots in Fig. 1 show that for ferritin, M_w = 780,000 g·mol^{-1}, $m = 1.30 \times 10^{-18}$ g, whereas, as expected, for apoferritin, M_w = 450,000 g·mol^{-1}.

Fig. 1 also shows that values of the second osmotic virial coefficients, A_2, for the two proteins are similar. This is not surprising: The A_2 values characterize the pair interactions between the solute molecules, determined by the identical surfaces of the molecules. The dynamic light-scattering results (see Fig. 5 and *Supporting Text*, which are published as supporting information on the PNAS web site, www.pnas.org) confirm the identical molecular size of the two proteins, $a = 13$ nm, equal to the crystallographic datum (14, 15); the latter equality also confirms the compliance of the diffusion of the two proteins to the Einstein–Stokes law of Brownian motion.

To quantify the crystallization kinetics of ferritin and apoferritin, we measured the growth rates of the layers on the surface of growing crystals using AFM (16, 18) and interferometry (25, 28). Fig. 2 shows that the proportionality between the step growth rate v and the crystallization driving force $[(C/C_e - 1) = (n/n_e - 1)]$ (C and n are the protein mass and molecular concentrations, $n = C/m$, respectively; the subscript e indicates their values at equilibrium with the crystal) is valid in a broad range of concentrations of both proteins. When the protein concentration is lower than the solubility, the steps retreat with a velocity symmetric to that in growth (see Fig. 2) as expected from the microscopic reversibility of the growth-dissolution processes (16, 18).

The values for n_e, determined from the data shown in Fig. 2 (16, 18) for ferritin and apoferritin are $(2.7 \pm 0.5) \times 10^{13}$ cm^{-3} and $(3.0 \pm 0.5) \times 10^{13}$ cm^{-3}, respectively. They are equal within the error limits, suggesting that the solubilities of these proteins do not depend on their molecular mass. In *Supporting Text* we provide statistical-mechanical arguments that indicate that this may be the case for protein molecules with near-spherical symmetry.

More importantly, Fig. 2 shows that at equal driving forces, the step growth rates are equal for the two proteins. The kinetic coefficient β, defined from refs. 6 and 12

$$v = \beta \Omega n_e (n/n_e - 1), \qquad [1]$$

with $\Omega = 1.56 \times 10^{-18}$ cm^3, the crystal volume per ferritin or apoferritin molecule, is $(6.0 \pm 0.4) \times 10^{-4}$ cm·s^{-1} for ferritin and $(6.0 \pm 0.3) \times 10^{-4}$ cm·s^{-1} for apoferritin. This is also equal to 6.0×10^{-4} cm·s^{-1}, which is the value for apoferritin extracted in refs. 16 and 18 from molecular-level AFM data.

Because similar values of the kinetic coefficient may result from completely different growth mechanisms, before we discuss the identical β values we need to establish the crystal growth mechanisms for the two proteins. Refs. 16 and 18 show for apoferritin that the steps grow by attachment/detachment of single molecules to kinks located along the steps. For ferritin, Fig. 3*a* illustrates the characteristic roughness of the growth steps. Fig. 3*b* shows the distribution of n_k, the number of molecules between the kinks, directly determined from several images similar to Fig. 3*a*. The mean $\bar{n}_k = 3.5$, corresponding to a mean kink density $\bar{n}_k^{-1} = 0.28$.

Fig. 3*c* shows a pseudoimage recorded with disabled scanning along the y axis such that the vertical coordinate becomes the time axis (16, 18). The figure of merit for the discussion here is the net growth of two molecules for 128 s, leading to an average net flux $(j_+ - j_-) = 0.054$ s^{-1} into the growth sites distributed with mean density $\bar{n}_k^{-1} = 0.28$.

Because there are no sources or sinks of molecules at the step other than the attachment sites, the step growth rate v should equal $a\bar{n}_k^{-1}(j_+ - j_-)$ (7, 12). At $(C/C_e - 1) = 1$, at which all data in Fig. 3 were collected, the value of the step growth rate from Fig. 2 is $v = 0.20$ nm·s^{-1}, equal to the product $a\bar{n}_k^{-1}(j_+ - j_-)$. This equality indicates that the step propagation in ferritin crystallization occurs only because of incorporation of molecules into the kinks along the steps. Thus, the propagation of ferritin steps follows the mechanism already established for apoferritin (16, 18). We conclude that the equality of the kinetic coefficients

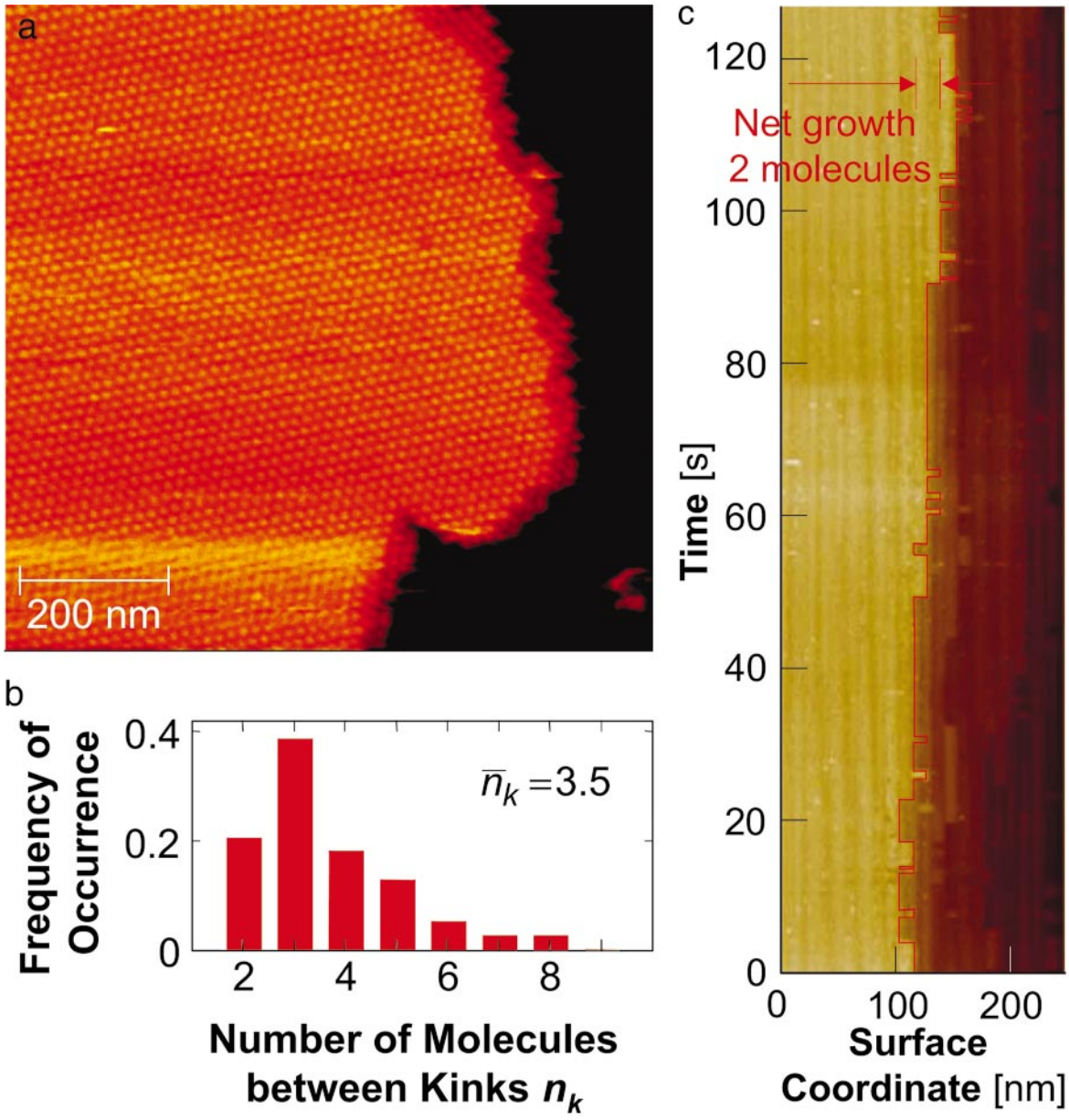

Fig. 3. The molecular mechanism of crystallization of ferritin. Brown and black, lower layer; ochre and orange, advancing upper layer. (*a*) Growth step at C = 70 μg·cm^{-3}, $(C/C_e - 1) = 1$. The contrast settings of this image, chosen to enhance the molecules in the upper layer, hide the molecules belonging to the lower layer on the right. (*b*) Distribution of molecules between kinks on steps located ≈0.5 μm apart, obtained from images similar to *a* at the same $(C/C_e - 1) = 1$. (*c*) Incorporation of molecules into steps at $(C/C_e - 1) = 1$. A pseudoimage recorded with the scan axis parallel to the step disabled at time = 0 (16, 18) shows the displacement of one molecular site at the step. In this imaging mode, the molecules in the upper and lower layers appear as vertical columns. The red contour traces step position. Left shifts of this contour indicate detachment of a molecule from the monitored site, and right shifts indicate molecular attachment into the monitored site. Tests similar to those described in refs. 16 and 18 show that this imaging mode does not affect the molecular attachment, and that the shifts of the monitored site are due to attachment and detachment of molecules either from the terrace between the steps or the adjacent solution rather than to one-dimensional diffusion of molecules along the step.

suggests that β does not depend on the mass of the crystallizing molecules.

This observation is in apparent contradiction with transition-state-type kinetic laws, in which the vibrational components of the transition-state partition function lead to proportionality of β to $m^{-1/2}$, characteristic i of transition-state kinetics discussed above. We conclude that the kinetics of incorporation into the kinks are limited only by diffusion.

For completeness, we now derive an expression for the kinetic coefficient of growth of crystals from solution as diffusion over an energy barrier, U, followed by unimpeded incorporation (1, 2). The barrier U may be of electrostatic origin (2); however, for the ferritin/apoferritin pair, it probably accounts for the need to expel the water molecules attached to the incoming molecules and to the growth site (29). Repulsive potentials due to water structuring at hydrophobic and hydrophilic surface patches can have significant strength and range (30, 31).

In Fig. 4 we schematically depict the resulting potential relief. The potential reaches its maximum value, U_{max}, at the crossing of the increasing branch, due to the repulsion between the incoming solute molecules and the crystal surface at

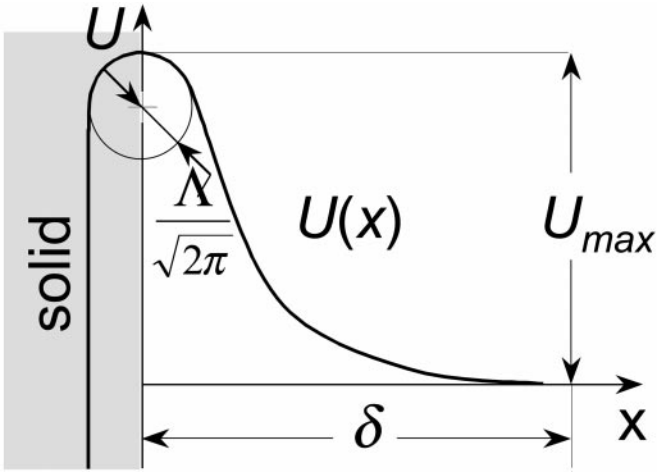

Fig. 4. A schematic illustrating the potential energy relief in front of the growth interface. For details, see the text.

medium separations, and the receding branch, which corresponds to the short-range attraction required if the molecules should enter the growth site. We position the beginning of the coordinate axis $x = 0$ at the location of this maximum. We assign a finite curvature of $U(x)$ about this maximum and link it with the expulsion of the last few solvent molecules as an incoming solute molecule joins the crystal. The finite curvature assumption follows previous solutions to similar problems (32, 33). The distance δ, used as the upper integration limit, is bound from below by the range of interaction of the solute molecules with the surface, which can be a few solute molecular sizes, and from above by the distances between the solute molecules in the solution bulk, $n^{-1/3} \approx 0.2\ \mu$m. Thus, δ can be chosen significantly longer than the molecular and kink sizes, and using a one-dimensional model is justified. Because the rate of diffusion over a sharp barrier only depends on the curvature around the maximum (32, 33), the choice of δ does not affect the result.

Because Brownian diffusion does not depend on the molecular mass, the above model yields a mass-independent kinetic coefficient (for details see *Supporting Text*). The resulting step growth rate v is

$$v = \frac{a}{\bar{n}_k}(j_+ - j_-) = \frac{a^3}{\bar{n}_k}\frac{D}{\Lambda}\exp\left(-\frac{U_{\max}}{k_B T}\right)(n - n_e), \qquad [2]$$

where Λ contains the radius of curvature of $U(x)$ around its maximum and hence is likely of the order of a few water-molecule sizes, ≈5–10 Å.

With $a^3 = \Omega$, we can rewrite Eq. **2** in the typical form of Eq. **1** that is readily comparable to experimental data. This defines β as

$$\beta = \frac{1}{\bar{n}_k}\frac{D}{\Lambda}\exp\left(-\frac{U_{\max}}{k_B T}\right). \qquad [3]$$

The parameters in this expression, $\bar{n}_k^{-1}$, D, Λ, and $U_{\max}$ have a clear physical meaning and can be measured independently.

For a consistency check, we substitute the values of $D = 3.2 \times 10^{-7}$ cm^2·s^{-1} (20) and $\Lambda = 10$ Å and get the experimentally determined value of β with $U_{\max} = 18$ kJ·mol^{-1} $= 7.3 k_B T$. This value is actually lower than the experimental barriers for ≈10 compounds centered around ≈28 kJ·mol^{-1} (13). Thus, the assumption of a diffusion-limited mechanism for ferritin and apoferritin allows a reasonable kinetic barrier, comparable with the effective activation energies of viscosity and diffusion in aqueous solutions (21, 34); a too-high barrier could indicate a slowly decaying transition state (2). Note that a proper determination of $U_{\max}$ would require knowledge about the growth mechanism, i.e., whether a solute molecule directly attaches to a growth site (6, 12), similar to the silver atoms during silver electrocrystallization (35), or, similar to potassium or ammonium dihydrogen phosphate (36–38), lysozyme (39), and canavalin (40), the molecules reach the growth sites after being adsorbed on the crystals surface (10).

The ratio $D/\Lambda\bar{n}_k$ has been used (41) as a kinetic coefficient for crystallization from the melt, with Λ defined as the "free path" of the building blocks, atoms or molecules, in the melt. In further work, this law was shown to poorly predict the behavior of metals during solidification (42). Note that in contrast to the above expression for melt growth, Eq. **3** treats growth from solutions with Einstein–Stokes diffusion of the solute molecules.

In a classical paper of Burton *et al.* (9), the ratio of the diffusivity to the mean distance between kinks, $D/a\bar{n}_k$, was used as a kinetic coefficient. This definition misses the energy barrier for growth, demonstrated by numerous later experiments (13). In a further development (10), the kinetic coefficients for motion of steps were postulated as $\beta = (D/\Lambda)\exp(-U/k_B T)$, with Λ introduced as a "jump length in the solution." Comparing this formula with our Eq. **3**, we see that Eq. **3** explicitly accounts for the mean kink density $\bar{n}_k^{-1}$ and provides a clear definition of Λ.

Evidence for diffusion-limited kinetics in other solution-crystallization systems can be found in experiments on growth of protein crystals in gels, where the protein diffusivity is significantly lower than in a "free" solution. It was found with two proteins that the maximum value of the growth rate, recorded at the early stages of growth before solution depletion and transport control set in, is 1.5–3 times lower than the equivalent value in free solutions (43). This suggests that the kinetic coefficient of growth is correlated to the diffusivity. In another work with the protein lysozyme, it was found that in gelled media, the protein concentration at the growth interface is essentially equal to the one in free solutions, whereas the concentration gradient at the interface, proportional to the growth rate, is lower by ≈1.5 times (44). This inequality is only possible if the kinetic coefficient in gels is lower, supporting the correlation between β and D and contradicting characteristic *ii* of the transition-state kinetic laws discussed above.

Furthermore, the known kinetic coefficients for crystallization of ≈12 proteins, protein complexes, and viri fit in the range of $0.8 - 20 \times 10^{-4}$ cm·s^{-1} (16, 28, 40, 45, 46). The molecular symmetry groups have orders ranging from 1 through 3 to 24 for the ferritins and 60 for the viri. No correlation exists between higher molecular symmetry and higher kinetic coefficients, which suggests that the rate-limiting step is not the decay of a transition state that should be facilitated for high-symmetry molecules with higher transition-state entropies (see characteristic *iii* discussed above).

To test whether the diffusion-limited kinetics also applies for phase transitions involving small-molecule substances, we consider the detailed data on the adsorption kinetics on the surface of a growing ammonium dihydrogen phosphate crystal (36, 37). The data for the temperature range 29–67°C were fitted to an equivalent of Eq. **3** with $\bar{n}_k^{-1} = 1$ to account for the suspected density of the adsorption sites (36, 37); for the surface diffusion mechanism selected by this system, adsorption is the process to be limited by either diffusion or a transition-state decay rate. The fit yielded $\Lambda = 13$ Å and $U = 27$ kJ/mol. The closeness of Λ to the range suggested above for the diffusion-limited case suggests that this mechanism is the rate-determining one for the investigated phase transition.

Further evidence in favor of the applicability of this mechanism to small molecules comes from the unusually narrow grouping of the kinetic barriers for growth of ≈10 diverse substances at 28 ± 7 kJ·mol^{-1} (13). The chemical nature of these substances ranges from inorganic salts through organic molecular compounds to proteins and viri. Hence, the narrow range of the activation barriers is unexpected for transition-state kinetics, where the activated complexes should reflect the chemical variety of the crystallizing compounds. On the other hand, assuming diffusion-limited kinetics, we note that the diffusivities in aqueous solutions have effective activation energies of ≈8–17 kJ·mol^{-1} (21, 34). If, as suggested by Eq. **3**, we subtract these values from the barriers of 28 ± 7 kJ·mol^{-1} (13) characterizing the overall kinetics, only ≈10–20 kJ·mol^{-1} remain for the barriers because of the interactions between the solute and the crystal surface. The above range of ±7 kJ·mol^{-1} is sufficiently broad to accommodate the chemical specificity of the solutes.

Thus, our experimental data in the context of other recent findings show that the kinetics of attachment of molecules to a growing phase during crystallization or other phase transitions in solution are diffusion-limited in many cases. This conclusion applies to proteins as well as to small-molecule systems. It is important to state once again that this result concerns the kinetics of incorporation of the solute molecules into existing attachments sites. In the cases where such sites are few or transport from the solution bulk is slow, the kinetics of creation of attachment sites or of transport may control the overall kinetics. What we argue is that after an attachment site exists and the solute molecules are standing in front of it, the rate of incorporation is solely limited by diffusion and not restricted by the decay of an intermediate state.

We thank J. J. DeYoreo for generously sharing unpublished results; O. Galkin and A. A. Chernov for numerous critical suggestions; B. R. Thomas for supplying purified proteins used in the experiments; and S.-T. Yau for help with the AFM imaging. Financial support was provided by the Office of Biological and Physical Research, National Aeronautics and Space Administration, and the National Lung, Heart, and Blood Institute, National Institutes of Health.

1. Smoluchowski, M. (1916) *Physik Z.* **17,** 557–585.
2. Eyring, H., Lin, S. H. & Lin, S. M. (1980) *Basic Chemical Kinetics* (Wiley, New York).
3. Neilsen, A. E. (1967) in *Crystal Growth*, ed. Peiser, S. (Pergamon, Oxford), pp. 419–426.
4. Kahlweit, M. (1969) in *Physical Chemistry*, ed. Eyring, H. (Academic, New York), Vol. VII, pp. 675–698.
5. Walton, A. G. (1969) in *Nucleation*, ed. Zettlemoyer, A. C. (Dekker, New York), pp. 225–307.
6. Chernov, A. A. (1961) *Sov. Phys. Uspekhi* **4,** 116–148.
7. Chernov, A. A. & Komatsu, H. (1995) in *Science and Technology of Crystal Growth*, eds. van der Eerden, J. P. & Bruinsma, O. S. L. (Kluwer, Dordrecht, The Netherlands), pp. 67–80.
8. Chernov, A. A. & Komatsu, H. (1995) in *Science and Technology of Crystal Growth*, eds. van der Eerden, J. P. & Bruinsma, O. S. L. (Kluwer, Dordrecht, The Netherlands), pp. 329–353.
9. Burton, W. K., Cabrera, N. & Frank, F. C. (1951) *Philos. Trans. R. Soc. London A* **243,** 299–360.
10. Gilmer, G. H., Ghez, R. & Cabrera, N. (1971) *J. Cryst. Growth* **8,** 79–93.
11. van der Eerden, J. P. (1994) in *Handbook of Crystal Growth*, ed. Hurle, D. (North–Holland, Amsterdam), Vol. 1a, pp. 307–476.
12. Chernov, A. A. (1984) *Modern Crystallography III, Crystal Growth* (Springer, Berlin).
13. DeYoreo, J. J. (2001) in *13th International Conference on Crystal Growth*, eds. Hibiya, T., Mullin, J. B. & Uwaha, M. (Elsevier, Kyoto).
14. Massover, W. H. (1993) *Micron* **24,** 389–437.
15. Harrison, P. M. & Arosio, P. (1996) *Biochim. Biophys. Acta* **1275,** 161–203.
16. Yau, S.-T., Thomas, B. R. & Vekilov, P. G. (2000) *Phys. Rev. Lett.* **85,** 353–356.
17. Yau, S.-T., Thomas, B. R., Galkin, O., Gliko, O. & Vekilov, P. G. (2001) *Proteins Struct. Funct. Genet.* **43,** 343–352.
18. Yau, S.-T., Petsev, D. N., Thomas, B. R. & Vekilov, P. G. (2000) *J. Mol. Biol.* **303,** 667–678.
19. Stranski, I. N. (1928) *Z. Phys. Chem. (Leipzig)* **136,** 259–278.
20. Petsev, D. N., Thomas, B. R., Yau, S.-T. & Vekilov, P. G. (2000) *Biophys. J.* **78,** 2060–2069.
21. Fredericks, W. J., Hammonds, M. C., Howard, S. B. & Rosenberger, F. (1994) *J. Cryst. Growth* **141,** 183–192.
22. Muschol, M. & Rosenberger, F. (1995) *J. Chem. Phys.* **103,** 10424–10432.
23. Choi, S. C. (1978) *Introductory Applied Statistics in Science* (Prentice–Hall, Englewood Cliffs, NJ).
24. Lin, H., Yau, S.-T. & Vekilov, P. G. (2003) *Phys. Rev. E Stat. Phys. Plasmas Fluids Relat. Interdiscip. Top.*, in press.
25. Vekilov, P. G., Monaco, L. A. & Rosenberger, F. (1995) *J. Cryst. Growth* **146,** 289–296.
26. Gliko, O., Booth, N. A., Rosenbach, E. & Vekilov, P. G. (2002) *Cryst. Growth Des.* **2,** 381–385.
27. Vekilov, P. G., Alexander, J. I. D. & Rosenberger, F. (1996) *Phys. Rev. E Stat. Phys. Plasmas Fluids Relat. Interdiscip. Top.* **54,** 6650–6660.
28. Vekilov, P. G., Thomas, B. R. & Rosenberger, F. (1998) *J. Phys. Chem.* **102,** 5208–5216.
29. Petsev, D. N. & Vekilov, P. G. (2000) *Phys. Rev. Lett.* **84,** 1339–1342.
30. Israelachvili, J. & Pashley, R. (1982) *Nature* **300,** 341–342.
31. Israelachvili, J. & Wennerstrom, H. (1996) *Nature* **379,** 219–225.
32. von Smoluchowski, M. (1918) *Z. Phys. Chem. (Leipzig)* **92,** 129–135.
33. Zeldovich, J. B. (1942) *J. Theor. Exp. Phys. (USSR)* **12,** 525–538.
34. Borchers, H. (1955) *Landolt–Bornstein Numerical Data and Functional Relationships, Materials Values, and Mechanical Behavior of Non-Metals* (Springer, Berlin), Vol. IV, Part II.
35. Bostanov, V., Staikov, G. & Roe, D. K. (1975) *J. Electrochem. Soc.* **122,** 1301–1305.
36. Vekilov, P. G., Kuznetsov, Y. G. & Chernov, A. A. (1992) *J. Cryst. Growth* **121,** 643–655.
37. Vekilov, P. G., Kuznetsov, Y. G. & Chernov, A. A. (1992) *J. Cryst. Growth* **121,** 44–52.
38. DeYoreo, J. J., Land, T. A. & Dair, B. (1994) *Phys. Rev. Lett.* **73,** 838–841.
39. Vekilov, P. G., Monaco, L. A. & Rosenberger, F. (1995) *J. Cryst. Growth* **156,** 267–278.
40. Land, T. A., DeYoreo, J. J. & Lee, J. D. (1997) *Surf. Sci.* **384,** 136–155.
41. Frenkel, J. (1932) *Phys. J. USSR* **1,** 498–510.
42. Broughton, J. Q., Gilmer, G. H. & Jackson, K. A. (1982) *Phys. Rev. Lett.* **49,** 1496–1500.
43. Garcia-Ruiz, J. M. & Moreno, A. (1997) *J. Cryst. Growth* **178,** 393–401.
44. Hou, W. B., Kudryavtsev, A. B., Bray, T. L., DeLucas, L. J. & Wilson, W. W. (2001) *J. Cryst. Growth* **232,** 265–272.
45. Malkin, A. J., Land, T. A., Kuznetsov, Y. G., McPherson, A. & DeYoreo, J. J. (1995) *Phys. Rev. Lett.* **75,** 2778–2781.
46. Malkin, A. J., Kuznetsov, Y. G., Glanz, W. & McPherson, A. (1996) *J. Phys. Chem.* **100,** 11736–11743.

Supporting Information for

Independence of the kinetics of solution-solid phase transition on the mass of the solute molecules

Dimiter N. Petsev, Kai Chen, Olga Gliko and Peter G. Vekilov

Characterization of the ferritin and apoferritin by dynamic light scattering

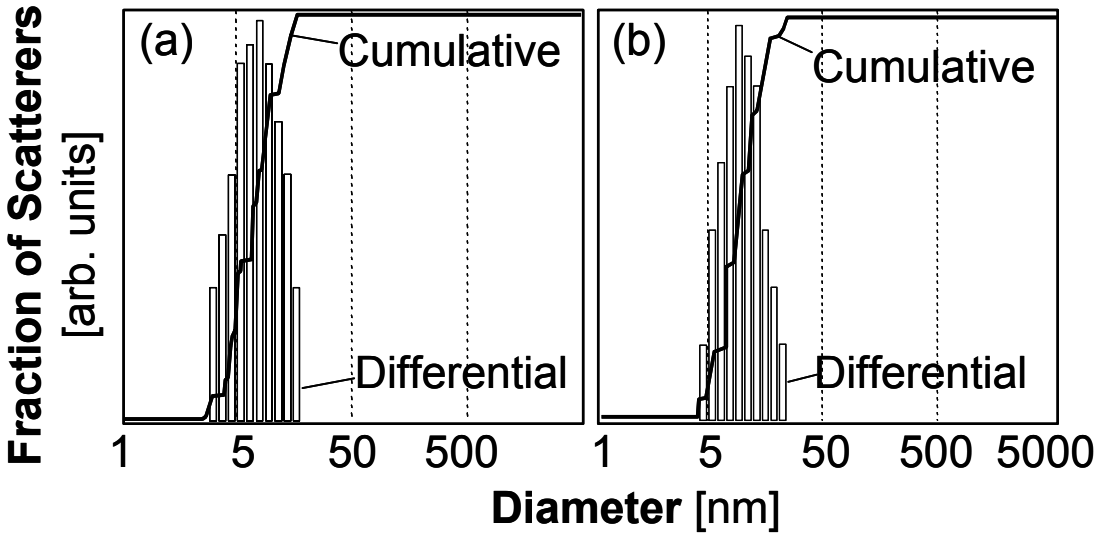

Fig. 5. Size distributions for (a) ferritin, and (b) apoferritin.

Fig. 5 displays the size distributions of the scatterers in solutions of the two proteins resulting from a dynamic light scattering determination as discussed in detail in Ref. (1). We see that the size distributions are narrow, and the two proteins have identical diameters of 13 nm. This is equal to their identical crystallographic diameters (2). Since these sizes are calculated from the set of experimentally-determined diffusivities using the Einstein-Stokes law of Brownian motion, the equality to the crystallographic data indicates that the diffusion of both molecules obeys this law (3).

Independence of solubility on molecular mass—statistical thermodynamics arguments

To rationalize the apparently equal solubility of ferritin and apoferritin, we consider the equilibrium between the solution and a crystal. This is equivalent to equilibrium between the states of a molecule in a kink on the crystal surface and in the solution (4-6). At constant temperature and pressure, the activity of a molecule in the crystal does not depend on the concentration of the solute and is equal to the activity of the standard crystal state (7, 8). Then, the equilibrium constant K_{cryst} can be written as

$$K_{\mathrm{cryst}} = (\gamma_e C_e)^{-1} = C_e^{-1} \qquad (1.)$$

where γ_e is the protein activity coefficient at a protein concentration equal to the solubility, and C_e is the solubility. The activity coefficient depends on the protein concentration and on the intermolecular interactions. Hence, we expect equal γ's in solutions of ferritin and apoferritin of equal concentration. Determinations of γ for apoferritin solutions of concentrations up-to 20-fold higher than the solubility have yielded $\gamma \cong 1$ (9). We expect the same to be true for ferritin, and this is the basis of the second equality above for these two proteins.

From the point of view of statistical thermodynamics, the equilibrium constant for crystallization K_{cryst} can be written as (10)

$$K_{cryst} = q_0 \exp(\mu_0 / k_B T) \quad , \qquad (2.)$$

where q_0 is the partition function of a molecule in a kink (which is only a function of temperature and pressure), μ_0 is the standard chemical potential of a molecule in the solution

To evaluate q_0 and μ_0, we assume that the internal molecular vibrations in the solution are the same as in the crystal and are decoupled from the other degrees of freedom. This allows us to neglect the internal vibrational partition function for both states. Furthermore, we limit ourselves to only translational contributions to the solute partition function, neglecting the rotational contributions, and those stemming from the intermolecular interactions. This limits the validity of the considerations below to molecules similar to the ferritin-apoferritin pair: with symmetry close to spherical, and that only exhibit very week intermolecular interactions and activity coefficient close to 1.

We do not take into account the contribution of the release or binding of the solvent molecules to the free energy changes of the phase transition. Although previous work has indicated that these contributions may be significant (9), we expect the contributions of the solvent effects to be identical for ferritin and apoferritin. This justifies neglecting them while aiming at comparisons between the two proteins. We also neglect the rotational vibrations in the crystal.

With these assumptions, we can use the expressions for the partition functions from Ref. (10), and write

$$q_0 = q_x q_y q_z \cong (q_{vib})^3 \tag{3.}$$

where q_i ($i = x, y, z$) is the partition functions for translational vibrations along the respective coordinate. In turn, with h-the Planck constant, ν-the vibration frequency, and U-the mean-force potential of a molecule in a kink,

$$q_{vib}=\frac{\exp\left(-\frac{h\nu}{k_BT}\right)}{1-\exp\left(-\frac{h\nu}{k_BT}\right)}\approx\frac{k_BT}{h\nu}\ , \qquad \nu=\frac{1}{2\pi}\sqrt{\frac{f}{m}}\ \text{, where } f=\left(\frac{\partial^2U}{\partial i^2}\right)_{\min}\ . \tag{4.}$$

Combining, we get for q_{vib} and q_0

$$q_{vib}=\frac{2\pi k_BT}{h}\sqrt{\frac{m}{f}}\ , \qquad q_0=\left(\frac{2\pi k_BT}{h}\right)^3\left(\frac{m}{f}\right)^{\frac{3}{2}}\ . \tag{5.}$$

For μ_0, we have (10)

$$\frac{\mu_0}{k_BT}=-\ln\left[\left(\frac{2\pi mk_BT}{h^2}\right)^{\frac{3}{2}}k_BT\right] \text{ and } \qquad \exp\left(\frac{\mu_0}{k_BT}\right)=\frac{1}{k_BT}\left(\frac{h^2}{2\pi mk_BT}\right)^{\frac{3}{2}}\ . \tag{6.}$$

Comparing the expressions for q_0 and $\exp(\mu_0/k_BT)$, we see that the former contains $m^{3/2}$, while the latter has $m^{-3/2}$, i.e., their product K_{cryst}, and C_e do not depend on the mass of the molecule.

It is important reemphasize two issues. (i) The thermodynamic considerations above are simplified and they only aim to address the issue of the equal solubility of two species that are identical in every respect but their mass. The equations above cannot be used to calculate values of thermodynamic functions. (ii) We did not account for the rotational degrees of freedom of the solute. This limits even this simplified model to molecules with close to spherical symmetry.

The flux of molecules into a kink

To calculate the flux J of molecules with concentration n that, driven by a concentration gradient, overcome a barrier to reach the surface, we orient the coordinate x perpendicular to a

growing surface and denote the potential relief close to this surface as $U(x)$. From the generalized Fick law, $J = (nD/k_BT)d\mu/dx$, with $\mu(T,x) = \mu_0(T) + k_BT\ln[\gamma\, n(x)] + U(x)$ and $\gamma \approx 1$ (9), J is linked to $U(x)$, $n(x)$ and the gradient of n as (11, 12)

$$J = D\left[\frac{dn(x)}{dx} + n(x)\frac{d\left(U(x)/k_BT\right)}{dx}\right] \quad , \quad x > 0 \, . \tag{7.}$$

with D being the Stokes diffusion coefficient of the molecules. In search of a steady $J = const$, we integrate the above equation with two sets of boundary conditions: (i) that at a certain distance from the surface δ, $x \geq \delta$, $U = 0$, and $n = n_\delta$; and, (ii) that in the crystal, i.e., at $x \leq 0$, $n = 0$.

Dividing by D and multiplying both sides by $\exp(U(x)/k_BT)$, we get

$$\frac{J}{D}\exp\left[U(x)/k_BT\right] = \frac{d}{dx}\left\{n(x)\exp\left[U(x)/k_BT\right]\right\} \tag{8.}$$

Integrating from $x = 0$ to $x = \delta$, using the boundary conditions at $x = 0$ and $x \geq \delta$, we get

$$J = \frac{n_\delta\, D}{\int_0^\delta \exp\left[U(x)/k_BT\right]dx} \quad , \tag{9.}$$

an analogue to Eq. (9.51) in Ref. (13) and the Fuchs expression for coagulation of particles interacting through $U(x)$.

If $U(x)$ has a sharp maximum at $x = 0$, we can represent it with a symmetric function around the point of the maximum. As shown below, in many cases $|d^2U/dx^2| < a$ and this justifies the assumption of a sharp maximum. We use only the first two members of its the Taylor series: $U(x) = U_{max} - \frac{1}{2}|d^2U/dx^2|\, x^2$. The minus sign stems from $d^2U/dx^2 < 0$ at the maximum. Then, the integral

$$\int_0^{\delta} \exp\left[U(x)/k_BT\right]dx = \exp\left(\frac{U_{\max}}{k_BT}\right)\int_0^{\delta}\exp\left[-\frac{1}{2}\left|\frac{\partial^2(U/k_BT)}{\partial x^2}\right|_{x=0} x^2\right]dx$$

$$\approx \exp\left(\frac{U_{\max}}{k_BT}\right)\int_0^{\infty}\exp\left[-\frac{1}{2}\left|\frac{\partial^2(U/k_BT)}{\partial x^2}\right|_{x=0} x^2\right]dx \quad . \qquad (10.)$$

$$= \exp\left(\frac{U_{\max}}{k_BT}\right)\left[\frac{2}{\pi}\left|\frac{\partial^2(U/k_BT)}{\partial x^2}\right|_{x=0}\right]^{-1/2}$$

The approximate equality above is based on $\delta >> [\frac{1}{2}|d^2U/dx^2|]^{-1/2}$, the half-width of the Gaussian function in Eq. (10.) Finally,

$$J = D\sqrt{\frac{2}{\pi k_BT}\left\{\left|\frac{\partial^2 U}{\partial x^2}\right|_{\max}\right\}^{1/2}} \exp\left(-\frac{U_{\max}}{k_BT}\right)n_{\delta} \quad . \qquad (11.)$$

Note that only half of the flux J from this equation contributes to growth: on top of the barrier, the force driving the molecules into the crystal is zero, and a molecule has equal chances of getting incorporated, or going back to the solution (14). With this, and introducing the parameter Λ as the radius of curvature of $U(x)/k_BT$ at its maximum:

$$\Lambda = \left(\frac{1}{2\pi}\left|\frac{\partial^2\left(U/k_BT\right)}{\partial x^2}\right|_{\max}\right)^{-1/2} , \qquad (12.)$$

the expression for J becomes

$$J = \frac{D}{\Lambda}\exp\left(-\frac{U_{\max}}{k_BT}\right)n_{\delta} \quad . \qquad (13.)$$

This last equation is essentially identical to the nucleation rate expression derived by Zeldovich (12) as a diffusion flux over a potential barrier in the space of cluster sizes.

If U_{max} is due to the hydration of the incoming molecule and the site where it attaches, the radius of curvature of $U(x)$ around U_{max} should be the size of a few water molecules, 2-4 Å, and the length Λ should be ~ 5-10 Å. Note that in this evaluation, we apply discreet considerations to a continuous model. Still, we expect the estimate of Λ to be roughly correct.

If all molecules that overcome the barrier are incorporated into a kink, the incoming flux into a kink is $j_+ = J\Delta S_{kink} \approx Ja^2$, where a^2 is an effective surface area of a kink. If there are no solute transport constraints (kinetic growth regime), n_δ is equal to that in the solution bulk n. Furthermore, in equilibrium, when n equals the solubility, n_e, $j_+ = j_-$. Since j_- does not depend on n in the solution, the step velocity v is

$$v = \frac{a}{\bar{n}_k}(j_+ - j_-) = \frac{a^3}{\bar{n}_k}\frac{D}{\Lambda}\exp\left(-\frac{U_{max}}{k_B T}\right)(n - n_e) \qquad (14.)$$

References.

1. Petsev, D. N., Thomas, B. R., Yau, S.-T. & Vekilov, P. G. (2000) *Biophysical J.* **78,** 2060-2069.
2. Lawson, D. M., Artymiuk, P. J., Yewdall, S. J., Smith, J. M. A., Livingstone, J. C., Trefry, A., Luzzago, A., Levi, S., Arosio, P., Cesareni, G., Thomas, C. D., Shaw, W. V. & Harrison, P. M. (1991) *Nature* **349,** 541-544.
3. Sun, S. F. (1994) *Physical Chemistry of Macromolecules* (John Wiley & Sons, New York).
4. Stranski, I. N. (1928) *Z. Phys. Chem.* **136,** 259-278.
5. Stranski, I. N. & Kaischew, R. (1934) *Z. Phys. Chem.* **B 26,** 100-113.
6. Kaischew, R. & Stranski, I. N. (1937) *Z. Phys. Chem.* **B35,** 427-432.

7. Eisenberg, D. & Crothers, D. (1979) *Physical Chemistry with Applications to Life Sciences* (The Benjamin/Cummins, Menlo Park).

8. Berry, P. S., Rice, S. A. & Ross, J. (2000) *Physical Chemistry* (Oxford University Press, New York).

9. Yau, S.-T., Petsev, D. N., Thomas, B. R. & Vekilov, P. G. (2000) *J. Mol. Biol.* **303,** 667-678.

10. Hill, T. L. (1986) *Introduction to Statistical Thermodynamics* (Dover, New York).

11. Smoluchowski, M. (1916) *Physik Z.* **17,** 557-585.

12. Zeldovich, J. B. (1942) *J. Theor. Experimen. Phys. (USSR)* **12,** 525-538.

13. Eyring, H., Lin, S. H. & Lin, S. M. (1980) *Basic Chemical Kinetics* (John Wiley and Sons, New York).

14. Zwanzig, R. (2001) *Nonequilibrium Statistical Mechanics* (Oxford University Press, Oxford).